Fuel 221 (2018) 407–416

Contents lists available at ScienceDirect

Fuel

journal homepage: www.elsevier.com/locate/fuel

Full Length Article

Dehydration of glucose to 5-hydroxymethylfurfural by a core-shell Fe_3O_4@SiO_2-SO_3H magnetic nanoparticle catalyst☆

Islam Elsayed[a,b], Mohammad Mashaly[b], Fathy Eltaweel[b], Michael A. Jackson[c], El Barbary Hassan[a,*]

[a] Department of Sustainable Bioproducts, Mississippi State University, Box 9820, Mississippi State, MS 39762, United States
[b] Department of Chemistry, Faculty of Science, Damietta University, Damietta 34517, Egypt
[c] United States Department of Agriculture, Agricultural Research Service, National Center for Agricultural Utilization Research, Renewable Products Technology Research, 1815 N. University St. Peoria, IL 61604, United States

GRAPHICAL ABSTRACT

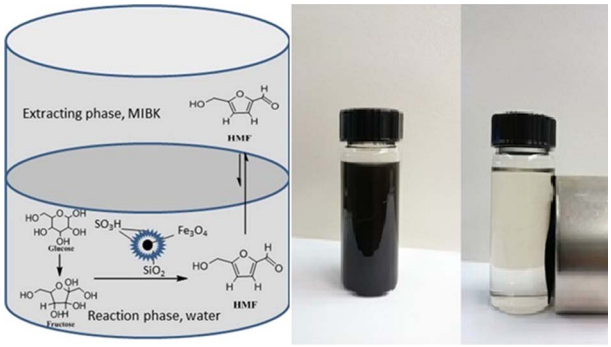

ARTICLE INFO

Keywords:
Glucose
Dehydration
5-Hydroxymethylfurfural
Magnetic nanoparticles
Fe_3O_4@SiO_2-SO_3H

ABSTRACT

In this paper we discuss the potential use of (Fe_3O_4@SiO_2-SO_3H) nanoparticle catalyst for the dehydration of glucose into 5-hydroxymethylfurfural (HMF). A magnetically recoverable (Fe_3O_4@SiO_2-SO_3H) nanoparticle catalyst was successfully prepared by supporting sulfonic acid groups (SO_3H) on the surface of silica-coated Fe_3O_4 nanoparticles. The prepared catalyst was characterized by FTIR, TGA, XRD, HRTEM-EDX, and N_2 adsorption-desorption isothermal analyses. The catalyst's surface acidity was determined by acid-base titration. Dehydration of glucose was performed in a biphasic system made up of water and methylisobutylketone (water/MIBK), and the effect of various reaction parameters affecting on the yield of HMF such as biphasic system ratio, catalyst concentration, temperature, time, and dimethylsulfoxide (DMSO) ratio were studied. Fe_3O_4@SiO_2-SO_3H catalyst disclosed a great catalytic activity for the formation of HMF and glucose conversion. About 70% yield of HMF and 98% glucose conversion were obtained at the optimum reaction conditions (40% catalyst concentration, 140 °C, 24 h and biphasic system of 1:4 (water: MIBK) ratio). At the end of the reaction, the catalyst was easily removed from the reaction mixture using a magnet and reused several times without high loss in catalytic activity.

☆ Mention of trade names or commercial products in this publication is solely for the purpose of providing specific information and does not imply recommendation or endorsement by the U.S. Department of Agriculture. USDA is an equal opportunity provider and employer.

* Corresponding author.
E-mail address: e.hassan@msstate.edu (E.B. Hassan).

https://doi.org/10.1016/j.fuel.2018.02.135
Received 13 September 2017; Received in revised form 19 February 2018; Accepted 20 February 2018
Available online 24 February 2018
0016-2361/

1. Introduction

Increasing energy demand and the existence of various problems associated with fossil fuels such as environmental pollution, global warming and diminishing petroleum reserves have greatly stimulated production of fuels and chemicals from renewable sources [1–3]. Lignocellulosic biomass has been considered as one of the potential sources for a variety of fuels and industrial chemicals [4,5]. HMF has been identified as an excellent platform molecule because it is a flexible intermediate for the synthesis of bio-renewable fuels and materials [6,7]. HMF can be converted to energy products such as 5-ethoxymethylfurfural [8], monomers for high-value polymers such as 2,5-furandicarboxylic acid [9], 2,5-hydroxymethylfuran [10]), and valuable intermediates for fine chemicals [11]. Therefore, extensive research about acid-catalyzed dehydration of carbohydrates to HMF has been performed [12–14].

Current feedstock resources of HMF production mainly includes cellulose, inulin, sucrose, glucose and fructose [15]. Some catalytic methods to produce HMF from glucose were reported in aqueous or organic media along with application of homogeneous and heterogeneous acids [16,17]. The use of organic solvents can provide many advantages and prohibit the formation of insoluble polymers and humins that can result from polymerization of carbohydrate degradation products. Also, the use of organic solvents can help to avoid the degradation of formed HMF into levulinic and formic acids as occurs in pure aqueous medium (acidified water) [18]. Dumesic and co-workers [6,19] have developed the use of biphasic reaction systems in which HMF formation can be enhanced in the aqueous phase (water) and simultaneously extracted by the organic solvent (organic phase). The use of biphasic system solves the problem of further conversion of produced HMF into undesirable levulinic or formic acid compounds through continuous extraction of furans into the organic phase. Biphasic solvents can also enhance the stabilization and yields of HMF product. Although heterogeneous catalysts are often recycled more easily than their homogeneous counterparts, the tedious recovery procedure via filtration or centrifugation and the inevitable loss of solid catalysts in the separation process still limited their application particularly for the small particle size.

Recently, magnetic nanoparticles based catalysts attracted more attention due to their good stability and easy separation from the reaction mixture by a permanent magnet [20,21]. The unique magnetic separation property makes MNPs much more effective than conventional filtration or centrifugation as it prevents loss of the catalyst. Several magnetic catalysts were successfully used for the conversion of biomass into chemicals and liquid fuels [22–24]. It has been demonstrated that the physical and chemical properties of the magnetic nanoparticles greatly depend upon the synthesis route [25]. To date, various techniques and different chemical synthetic methods for preparing magnetite (Fe_3O_4) nanoparticles (MNPs) already have been reported, such as co-precipitation, micro-emulsions, solvothermal processing, and high-temperature organic phase decomposition [26–28]. However, MNPs are readily aggregated due to electrostatic and magnetic attractions that can produce clusters. In order to prevent the aggregation, the surface of MNPs can be modified with various kinds of materials, including polymers [29], noble metals [30] and silica [31]. Among them, silica is considered to be one of the most promising candidates because it not only protects MNPs from oxidation and agglomeration, but it is also compatible with various chemicals and molecules for bio-conjugations due to its unique surface chemistry [32]. Currently, the Stöber method [33] and microemulsion method [34] are the most common approaches for silica coating. Zehui et al. prepared silica-coated MNPs supported phosphotungstic acid catalyst for the synthesis of 5-ethoxymethylfurfural from 5-hydroxymethylfurfural and fructose[35]. Zehui and his coworkers also used silica-coated MNPs supported sulfonic acid (SO_3H) catalyst successfully for the hydrolysis of cellulose in ionic liquids at low temperatures 70–100 °C [36]. It is well known that strong acid catalysts such as sulfuric or sulfonic acids can be used successfully for both hydrolysis and dehydration reactions. Wang et al. successfully used sulfonic acid-functionalized mesoporous carbon catalyst (OMC-SO_3H) for efficient conversion of fructose into 5-hydroxymethylfurfural and 5-ethoxymethylfurfural [37]. However, there was no previous studies discussed the ability of using silica coated MNPs supported sulfonic acid (SO_3H) as catalyst for the dehydration of sugars to furan derivatives. Due to the advantages of both magnetic nanoparticles acid catalysts and biphasic system, the purpose of this research is to study the effectiveness of silica coated MNPs supported with sulfonic acid groups (Fe_3O_4@SiO_2-SO_3H) on the dehydaration of glucose to HMF. For this purpose, this catalyst was prepared by immobilization of sulfonic groups (SO_3H) on the surface of silica-coated magnetite (Fe_3O_4@SiO_2) nanoparticles. The prepared catalyst was characterized by FTIR, TGA, XRD, HRTEM-EDX, N_2 adsorption-desorption analyses, and acid base titration. The factors affecting on the yield of HMF such as time, temperature, solvent composition, catalyst loads, and dimethylsulfoxide (DMSO) ratio were also studied.

2. Experimental

2.1. Materials

Ferric chloride hexahydrate (≥99%), 1-octadecene (technical grade 90%), polyoxyethylene (5) nonylphenylether (Igepal CO-520), tetraethyl orthosilicate (TEOS, reagent grade 98%), Oleic acid (technical grade 90%), chlorosulfonic acid (99%), formic acid (reagent grade ≥ 95%), 5-hydroxymethylfurfural (HMF, 99%), anhydrous hexane (95%) and anhydrous sodium hydroxide (pellets ≥ 99%) were purchased from Sigma-Aldrich. Dimethyl sulfoxide (DMSO, 99.5%), cyclohexane, ammonium hydroxide (reagent grade 29% by weight), ethanol and methanol were purchased from Fischer Scientific. Methyl isobutyl ketone (MIBK 99.5%), heptane, acetonitrile for HPLC and sulfuric acid (extra pure 96%) were purchased from Acros. D-glucose (≥99%), fructose, and levulinic acid were obtained from Alfa Aesar. High purity water (17.8 megohm-cm) was purified through Thermo Scientific E-pure Water purification system. All chemicals were used as-received without further purification.

2.2. Preparation of the catalyst

2.2.1. Preparation of Fe_3O_4 NPs

Fe_3O_4 NPs were synthesized according to the method described by Park et al. [38]. In a typical preparation procedure, 10.8 g of ferric chloride hexahydrate were dissolved in a solvent mixture composed of 120 mL deionized water, 160 mL ethanol, and 280 mL hexane. Then 38 mL oleic acid were added to the previously prepared solution and stirred at room temperature for 30 min. 4.8 g sodium hydroxide were added to the resulting solution and stirred in a closed reactor at 70 °C for 4 h. By using a separating funnel, the formed solution was separated into two different layers. The upper organic layer containing ferric oleate complex was collected and washed three times with deionized water. After washing, hexane was evaporated off overnight at 80 °C. The sticky ferric oleate precursor was dispersed in 6.4 mL of oleic acid and 250 mL of 1-octadecene. The mixture was degassed with helium for 30 min at room temperature. The reactants were kept at 100 °C for one hour to remove the residual solvents before heating up to 320 °C, then, the temperature was kept at 320 °C for 2.5 h under helium flow. The solution was cooled to room temperature and precipitated by addition of excess ethanol, the precipitate was collected by centrifugation and the supernatant decanted. The isolated solid Fe_3O_4 NPs was re-dispersed in heptane and then precipitated with ethanol. The precipitation and re-dispersion process was repeated several times to purify the prepared iron oxide NPs and then dried overnight via vacuum drying.

2.2.2. Preparation of $Fe_3O_4@SiO_2$ NPs

$Fe_3O_4@SiO_2$ core − shell nanoparticles were prepared by using a reverse microemulsion method. 100 g of Igepal CO-520 was dispersed in 200 mL of cyclohexane and sonicated for 15 min. Then, 0.5 g of Fe_3O_4 nanoparticles was added to the above solution with continuous stirring. Thereafter, 80 mL of ammonium hydroxide were added to the above mixture solution. Finally, 112 mL of tetraethyl orthosilicate were added via three fractionation drop systems with mechanical stirring. The resulting $Fe_3O_4@SiO_2$ core − shell nanoparticles were separated by centrifugation and collected by a permanent magnet, and rinsed repeatedly with deionized water until the filtrate was no longer alkaline. Lastly, $Fe_3O_4@SiO_2$ nanoparticles were washed with ethanol three times and dried overnight via vacuum drying.

2.2.3. Preparation of ($Fe_3O_4@SiO_2$-SO_3H) NPs

The magnetic acid catalyst ($Fe_3O_4@SiO_2$-SO_3H) was prepared in a similar way that was used for the preparation of silica supported sulfonic acids [39]. Typically, 0.45 g of $Fe_3O_4@SiO_2$ were charged into a 500 mL Büchner flask, which was equipped with a constant pressure dropping funnel and a gas inlet tube for conducting of HCl gas over an adsorbing solution of NaOH. Then, chlorosulfonic acid (0.1745 g mol) was added dropwise over a period of 30 min at room temperature. After the addition was completed, the resulting mixture was shaken for 30 min. Then the catalyst $Fe_3O_4@SiO_2$-SO_3H was washed successively with ethanol, and dried overnight via vacuum drying.

2.3. Catalyst characterization

X-ray diffraction (XRD) patterns were recorded with RINT Ultima III XRD (Rigaku Corp., Japan) operating with CuKα1 radiation (λ = 1.54 Å) at 40 KV 44 mA. Samples were ground and measured on deepened glass sample holders. High resolution transmission electron microscope equipped with an energy dispersive X-ray spectroscopy (HRTEM/EDX) images were obtained using JEOL 2100 TEM with LaB6 emitter operated at 200KV. Samples were grounded and dispersed in ethanol and a drop of this suspension deposited on a 300 mesh Formvar carbon coated Cu grid and allowed to dry overnight before Imaging. The Fourier Transform Infrared (FTIR) spectroscopy performed by Thermo Scientific Nicolet iS50 FTIR spectrometer in the range of 500–4000 cm^{-1}. Thermal gravimetric analysis (TGA) was determined by using Thermo Scientific SDT Q600 series Thermogravimetric Analyzer (TA instrument) and all sample runs were performed at heating rate 10 °C/min from 25 °C to 550 °C under nitrogen atmosphere at flow rate 100 mL/min. Surface areas and pore volumes of *Fe_3O_4*, *$Fe_3O_4@SiO_2$*, and *$Fe_3O_4@SiO_2$-SO_3H* nanoparticles were determined by adsorption-desorption isotherms of nitrogen at − 196 °C by a Quantachrome Autosorb iQ gas sorption analyzer (Quantachrome, USA). Prior to undergoing gas adsorption measurements, specimens were degassed at 105 °C under a vacuum for a period of 3 h. The apparent surface area of nanoparticles was calculated by the BET method. The total pore volume was determined by converting nitrogen gas adsorbed at a relative pressure of 0.99 to the volume of liquid adsorbate (nitrogen).

2.4. Catalyst titration

Acid-base titrations were used to measure the acidity of both fresh and spent $Fe_3O_4@SiO_2$-SO_3H acid catalysts. 0.01 g of each catalyst was suspended in 30 mL water/ethanol (2:1) by using mechanical stirrer and titrated against 0.01 M NaOH solution. The pH of the solution was measured by Thermo Scientific Orion 4 Star plus Ph/ISE Benchtop Multiparameter Meter.

2.5. Biphasic conversion of glucose to HMF

Conversion experiments were performed in a 70 mL stainless steel reactor. Biphasic solution consisting of 5 mL of 10% aqueous glucose solution with 15, 20 or 25 mL of MIBK, and $Fe_3O_4@SiO_2$-SO_3H catalyst (20–75%) were placed in the reactor and mixed together. The percentage of the catalyst in each run was calculated based on the volume of glucose solution in the biphasic system (5 mL). The reactor was then immersed in a preheated oil bath connected with temperature controller and heater, this time was considered to be the starting reaction time. Conversion experiments were performed at four different temperatures (110, 120, 130, and 140 °C) and different reaction times (6, 12, 18, 24, 30, and 36 h). Experiments with optimum conditions were repeated by adding dimethyl sulfoxide (DMSO) to the aqueous glucose/MIBK biphasic system. The total volume of aqueous glucose solution and DMSO was kept constant (5 mL) for each composition and the ratios of aqueous glucose solution to DMSO was 8:2, 7:3, 6:4, 5:5 and 4:6. After each run, the biphasic solution was filtered with Whatman 42 filter paper to separate any solid particles from the solution. The filtered biphasic solution was poured into a measuring cylinder to determine the volume of both organic and aqueous layers. The two layers were separated by using separating funnel, and filtered again with 0.2 µL syringe nylon membrane (Millex-GN). HMF was detected in both organic and aqueous layer by HPLC.

2.6. Analysis of glucose and HMF

Both aqueous and organic filtrates were analyzed by 1100 Agilent High Performance Liquid Chromatography (HPLC) equipped with ZORBAX eclipse plus C18 (5 µm, 4.6 × 150 mm) column and UV detector. During this process, the column temperature remained constant at 30 °C, and the mobile phase was methanol–water (1:5 v/v acidified by 5% acetic acid) at flow rate of 1 mL/min with UV detection at 282 nm. 10 µL of each sample was injected and the concentration of HMF was calculated based on standard calibration curve obtained with standard prepared solutions of HMF. The concentration of unreacted glucose and formed fructose were analyzed by high performance liquid chromatography (HPLC) using Agilent 1200 instrument equipped with a refractive index detector and Bio-Rad Aminex HPX-87H ion Exclusion Column (7.8 mm × 300 mm) at 60 °C. The sample was analyzed with 0.005 mol/L sulfuric acid as eluent at flow rate of 0.6 mL/min for 35 min.

2.7. Catalyst recycling

After reaction, $Fe_3O_4@SiO_2$-SO_3H catalyst was removed from the reaction mixture using a permanent magnet. Then the catalyst was washed carefully with 25 mL of ethanol/water to remove any traces from MIBK and dried at 105 °C in a vacuum oven overnight. The conversion experiments using the recycled catalyst were performed at the optimum experimental conditions.

2.8. Calculations

HMF yield and glucose conversion were calculated by the following equations:

$$Yield\ \% = \frac{[HMF]aq \times [V]aq + [HMF]org \times [V]org}{[glucose]feed \times [V]feed} \times \frac{180}{126} \times 100 \quad (1)$$

$$Conversion\ \% = \frac{[glucose]feed \times [V]feed - [glucose]aq \times [V]aq}{[glucose]feed \times [V]feed} \times 100 \quad (2)$$

where “feed”, ”aq” and “org” are representing the initial phase, aqueous phase and organic phase, respectively; [glucose] and [HMF] were the finial concentration of sugar and HMF in solution, respectively, [V] Volume of solution, and “180” and “126” are the molecular weights for glucose and HMF, respectively.

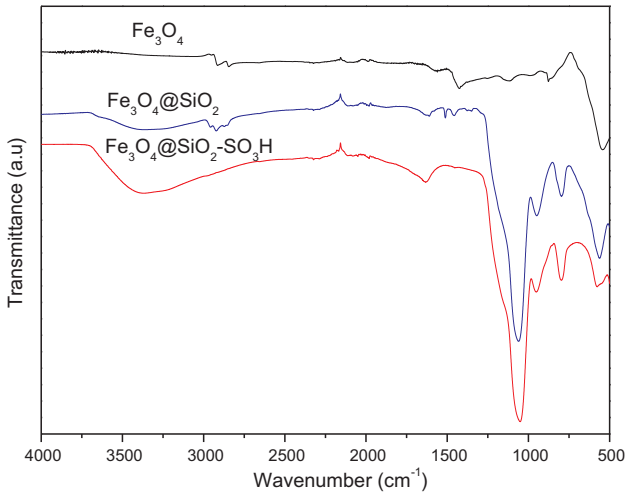

Fig. 1. FTIR spectra of magnetite nanoparticles Fe_3O_4, $Fe_3O_4@SiO_2$ and $Fe_3O_4@SiO_2$-SO_3H.

3. Results and discussion

3.1. Catalyst characterization

FTIR analysis is an important tool to identify the functionalization and coating layers on the surface of the magnetite nanoparticles. Fig. 1 shows FTIR spectra for the prepared magnetite nanoparticles Fe_3O_4, $Fe_3O_4@SiO_2$ and $Fe_3O_4@SiO_2$-SO_3H. In the FTIR spectra of Fe_3O_4, the two absorption bands at 2903 and 2840 cm^{-1} are attributed to the asymmetric and symmetric CH_2 stretching of the trace amounts of organic solvent. The absorption band at 547 cm^{-1} corresponds to Fe-O bending vibrations [28,33,35,36]. FTIR spectra of $Fe_3O_4@SiO_2$ nanoparticles show two weak absorption bands at 3354 and 1609 cm^{-1} due to the O-H stretching and bending vibrations of the adsorbed water on silica surface. The broad high-intensity band at 1060 cm^{-1} can be attributed to Si-O-Si asymmetric stretching vibrations. The band at 795 cm^{-1} was assigned to Si-O-Si symmetric stretching vibration of the rocking mode of Si-O-Si. The sharp band at 430 cm^{-1} represents an extra evidence for Si-O-Si or O-Si-O bending vibrations mode. The presence of Si-OH symmetric stretching vibration was also confirmed by the absorption band at 950 cm^{-1}. FTIR spectra of $Fe_3O_4@SiO_2$-SO_3H nanoparticles show two characteristic adsorption bands at 3354 and 1609 cm^{-1} related to the O=H stretching and bending vibrations of SO-H bond of the sulfonic acid group (SO_3H). The FTIR absorption range of the O=S=O asymmetric and symmetric stretching modes were observed at 1175 and 1051 cm^{-1} and located at the same vibration band of Si-O-Si group [40]. The S-O stretching vibration was observed at 579 cm^{-1}. FTIR spectra clearly indicated that the surface of $Fe_3O_4@SiO_2$ was successfully functionalized with sulfonic acid groups.

The presence of SiO_2 and SiO_2-SO_3H layers on the surface of the magnetite (Fe_3O_4) nanoparticles was confirmed by TGA/DTA measurements. Fig. 2 shows the different stages of weight loss for Fe_3O_4, $Fe_3O_4@SiO_2$ and $Fe_3O_4@SiO_2$-SO_3H nanoparticles from room temperature to 600 °C. $Fe_3O_4@SiO_2$-SO_3H catalyst shows four steps of weight loss in the following temperature ranges: 25–120 °C, 120–320 °C, 320–490 °C and more than 490 °C. In the TGA curve of magnetite (Fe_3O_4) nanoparticle, the decreasing in weight (1.8%) from room temperature to 120 °C was caused by the removal of adsorbed water and any traces organic solvents from the sample [41]. The second weight reduction (3.5%) in the range from 120 to 320 °C may be attributed to the evaporation and subsequent decomposition of SO_3H groups as SO_3 gas [42,43]. Other studies [44–46], suggested that the weight reduction in the prior range was corresponded to the removal of free oleic acid from Fe_3O_4 nanoparticles. In fact, we disagree with the above suggestion because Fe_3O_4 magnetite nanoparticles were prepared by thermal decomposition at higher temperature (320 °C) for the long period of time of 2.5 h. The magnetite nanoparticles preparation temperature was much higher than the decomposition temperature of oleic acid (b.p., 194–195 °C/1.2 mmHg). In addition, FTIR spectra of magnetite (Fe_3O_4) nanoparticles agrees with our explanation because there is no peak at 1710 cm^{-1} belonging to the carboxylic group of oleic acid. The third weight loss (8.7%) in the range from 320 to 490 °C was resulted from the decomposition of silica shell [42]. The weight drop after 570 °C is likely due to the phase transition from Fe_3O_4 to FeO. The phase diagram of the Fe-O system indicates that FeO is the most stable species at temperatures above 570° [44]. The general shapes and percentage of weight losses for magnetite and SiO_2 coated magnetite are very similar indicating that the silica coated film is thermally stable. The percentages of weight loss for SiO_2 coated magnetite at ranges 25–120 and 120–490 were 4.3% and 17.7%, respectively, and the residual mass was 78.0% at 600 °C.

The morphological structure for the synthesized $Fe_3O_4@SiO_2$-SO_3H nanoparticles was characterized by HRTEM. The elemental analysis was performed by EDX equipped with TEM. The presence of silicon and sulfur peaks in the quantitative EDX analyses of both fresh and spent $Fe_3O_4@SiO_2$-SO_3H catalysts indicate successful functionalization for SiO_2 and –SO_3H groups on the surface of Fe_3O_4 core-shell (Fig. 3a and b). HRTEM images of both fresh and spent $Fe_3O_4@SiO_2$-SO_3H catalysts clearly confirm the presence of the (SiO_2) and (SO_3H) group coated layers on the surface of the catalyst (Fig. 3c and d). The outer, coated layer of the spent catalyst appears to be rougher than that in the fresh catalyst and this may be related to the partial leaching of SO_3H group. Fig. 3a and b clearly indicates that about 22% of the sulfur was leached from the spent catalyst after five runs.

The acidity of both fresh and spent $Fe_3O_4@SiO_2$-SO_3H catalyst after five runs was determined by acid-base titration method as shown in Fig. 4. This method is based on the changing of pH value with increasing the amount of NaOH standard solution. The initial pH values of fresh and spent $Fe_3O_4@SiO_2$-SO_3H catalysts were 3.6 and 4.2, respectively. Furthermore, the number of H^+ sites in fresh and spent $Fe_3O_4@SiO_2$-SO_3H catalysts were determined to be about 2.5 and 2.25 mmol/g, respectively. This result confirms the deactivation and partial leaching of SO_3H group from the surface of the spent catalyst as indicated in Fig. 3a and b.

Generally, XRD can be used to characterize the crystallinity of a nanoparticle and it gives the average diameters for all nanoparticles. The XRD patterns of the Fe_3O_4 and $Fe_3O_4@SiO_2$-SO_3H are shown in Fig. 5. A series of characteristic peaks were observed in the XRD pattern at 2θ of 30.2°, 35.6°, 43.2°, 53.9°, 57.3°, 62.9° and 74.7° 2θ corresponding to the diffractions of [2 2 0], [3 1 1], [4 0 0], [4 2 2], [5 1 1], [4 4 0] and [5 2 2] crystal planes of a cubic spinel unit cell which match well with the standard Fe_3O_4 pattern [47]. The peak broadening of XRD pattern indicates the significantly small size of the resulting crystallites. According to the peak widths, the average crystallite size of Fe_3O_4 nanoparticles was estimated using Scherrer's formula to be 12.9 nm, this result is in good agreement with the value 13.3 nm of the mean particle sizes determined by TEM images. There are no peaks for any other phases that were observed in the XRD patterns which indicate high purity of the product. The black color of the powder further verifies that it is mainly in the magnetite phase and not maghemite (brown) of the same spinel structure. All the previous characterization techniques (FTIR, TGA, HRTEM-EDX and acid titration) confirmed the presence of SiO_2-SO_3H layers on the surface of the magnetite (Fe_3O_4) nanoparticles. However, XRD didn't show any remarkable diffraction peaks for SiO_2-SO_3H layers; because, the diffraction patterns for both Fe_3O_4 and $Fe_3O_4@SiO_2$-SO_3H are exactly the same. This result suggests the presence of SiO_2-SO_3H amorphous shells on the surface of Fe_3O_4 core are too thin to be measured using XRD [33,48].

To get a clear view of the surface area and porous nature of the prepared magnetic nanoparticles, a nitrogen adsorption-desorption

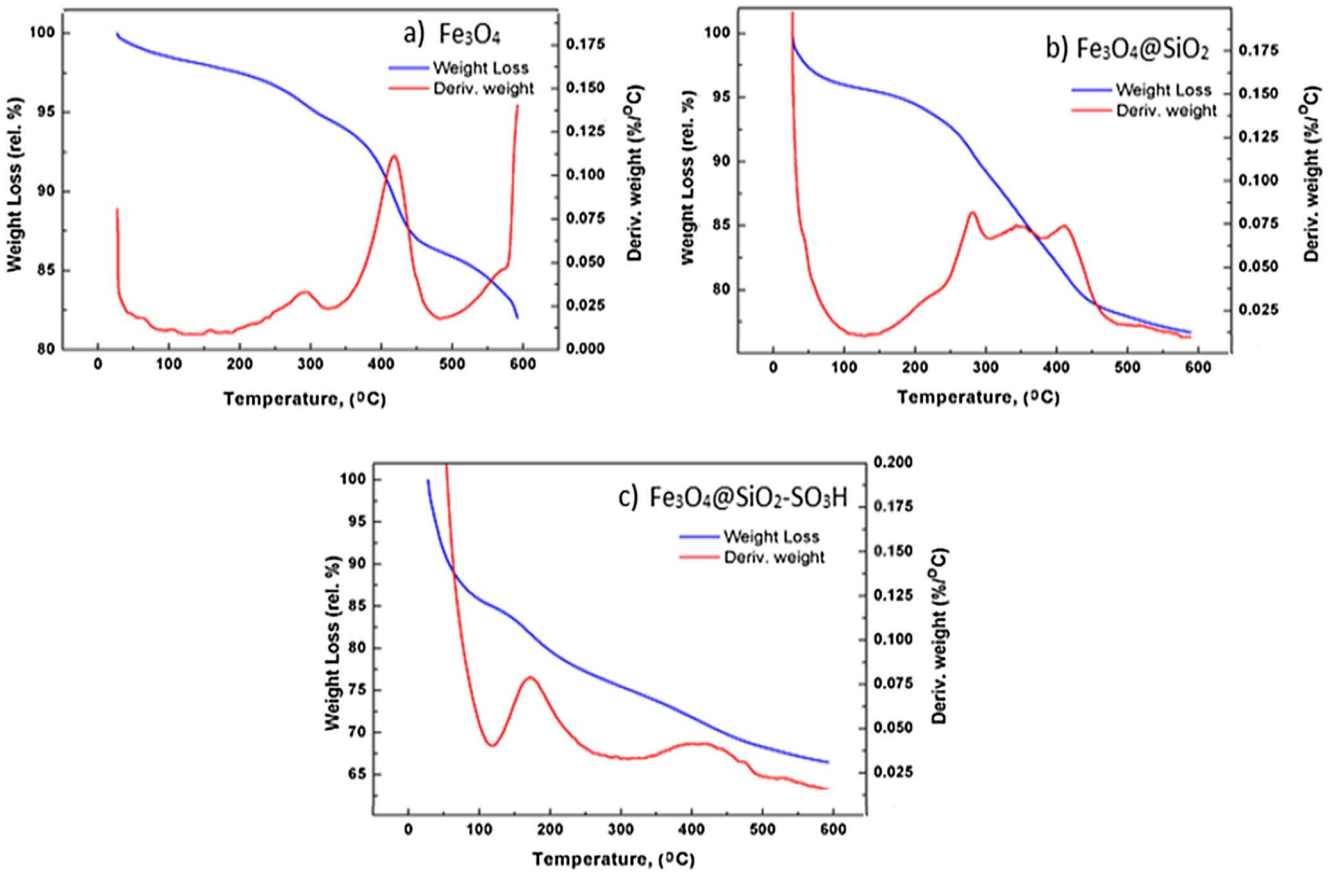

Fig. 2. TGA curves of a) Fe_3O_4, b) Fe_3O_4@ SiO_2, and c) Fe_3O_4@ SiO_2-SO_3H nanoparticles.

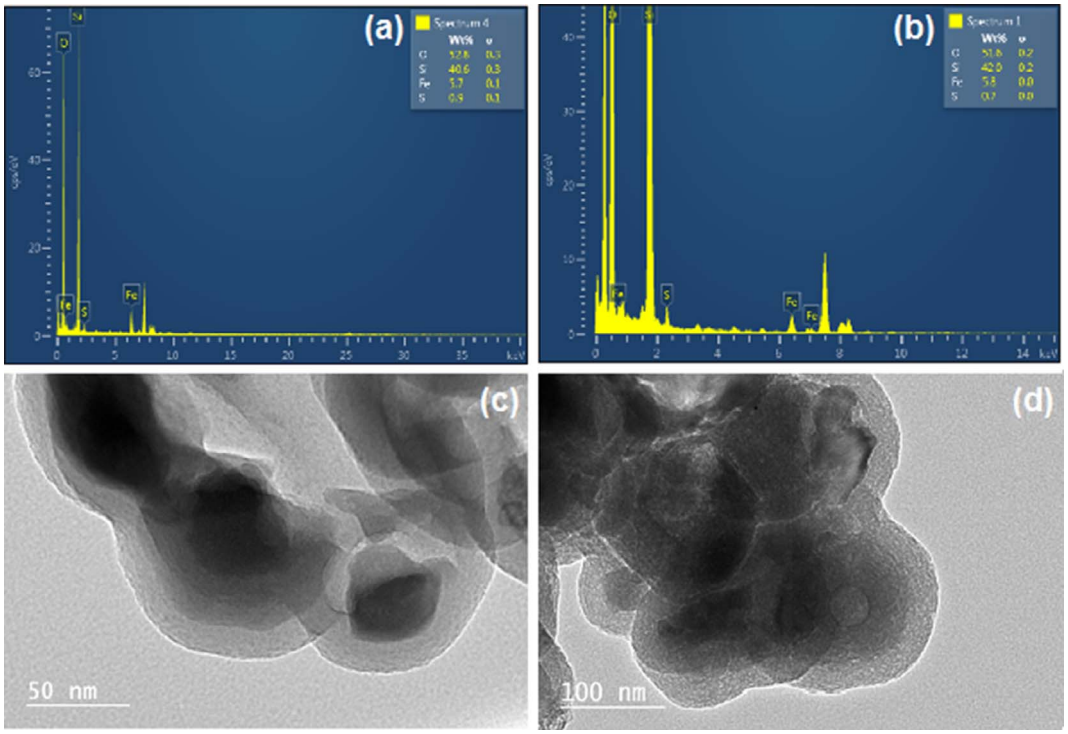

Fig. 3. (a) EDX of fresh Fe_3O_4@SiO_2-SO_3H, (b) EDX of spent Fe_3O_4@SiO_2-SO_3H, (c) HRTEM of fresh Fe_3O_4@SiO_2-SO_3H, and (d) HRTEM of spent Fe_3O_4@SiO_2-SO_3H catalyst (after 5 runs).

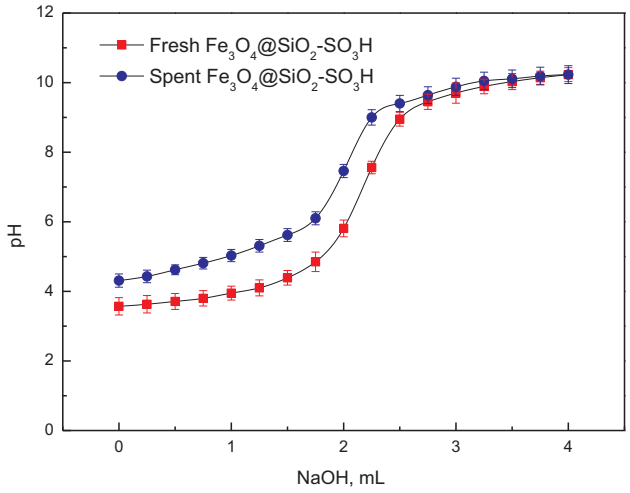

Fig. 4. Acid-base titration curves of fresh and spent Fe_3O_4@SiO_2-SO_3H catalyst after 5 runs.

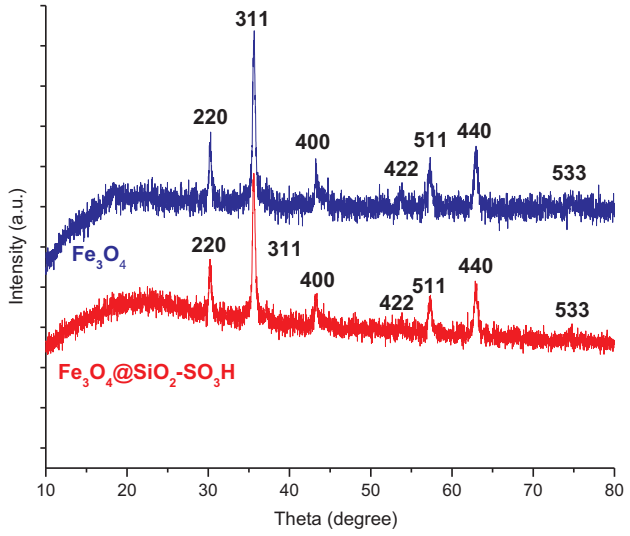

Fig. 5. XRD patterns of the Fe_3O_4 and Fe_3O_4@SiO_2-SO_3H.

isotherm was used to determine the catalyst texture structure. As shown in Fig. 6a, the isothermal of Fe_3O_4@SiO_2-SO_3H behaved as a typical type IV adsorption isotherm indicating a mesoporous structure for the catalyst. BJH values of surface area, pore size, and pore radius are presented in Fig. 6b. Results indicated that our targeted prepared magnetic nanocatalyst (Fe_3O_4@SiO_2-SO_3H) possessed surface area ($106.8\ m^2/g$) comparable to the previously reported value ($93.3\ m^2/g$) for the same catalyst [49]. The prepared catalyst also possessed an average pore size of (3.7 nm) and pore volume of (0.474 cc/g).

3.2. Isomerization and dehydration mechanism of glucose

It is generally accepted that glucose isomerization to fructose, and fructose dehydration to HMF require the presence of both Brönsted and Lewis acid sites [50,51]. Scheme 1 shows the proposed reaction mechanism for the formation of HMF via isomerization and dehydration of glucose [52]. The presence of fructose in the aqueous phase as shown in the Supplementary Fig. (S3) indicating that the mechanism of the reaction proceeded through the isomerization of glucose to fructose. The partial agglomeration of Fe_3O_4 magnetite nanoparticles due to its strong magnetism, even in the presence of dispersing agent, prevent 100% coating of Fe_3O_4 with silica and consequently SO_3H groups. At higher temperatures, some of the agglomerated Fe_3O_4 particles (partially coated) can be separated from each other and the uncoated parts acting as Lewis acid to initiate isomerization of glucose to fructose. Sulfonic acid (SO_3H) group on the surface of Fe_3O_4@SiO_2-SO_3H catalyst acts as Brönsted acid to dehydrate fructose into HMF.

3.3. Effect of MIBK ratio on glucose dehydration process

Recently, the dehydration of carbohydrates into HMF by heterogeneous catalyst was performed in a water/MIBK [53], water/butanol [54] or water/butanone biphasic systems. Water/MIBK biphasic system significantly gave higher yield and selectivity than water/butanol and water/butanone biphasic systems. According to the literature [33], MIBK is a good solvent that could suppress unwanted side reactions in glucose dehydration in water using acid catalysts, and could extract more HMF into organic phase with good partitioning of HMF compared to other solvents. So, MIBK and water biphasic system was used in this study to evaluate the catalytic activity of Fe_3O_4@SiO_2-SO_3H catalyst. The reactivity of glucose towards dehydrations was tested in three different ratios of water/MIBK biphasic system (1:3, 1:4, and 1:5) in presence of Fe_3O_4@SiO_2-SO_3H catalyst. Fig. 7 shows the influence of water/MIBK ratio on the yield and conversion of HMF. As shown in the figure, the yield of HMF slightly increased from 69.6% at (1:3) ratio to 70.5% at (1:4) ratio. Further increase in the water/MIBK ratio to (1:5) did not improve the yield of HMF. At the same time, changing water/MIBK ratio did not show any significant effect on the conversion percentage of HMF. Accordingly, water/MIBK ratio of (1:4) was chosen as the optimum ratio in this biphasic system for the rest of experiments.

3.4. Effect of catalyst concentration on glucose dehydration process

Concentration and nature of a catalyst play an important role on the

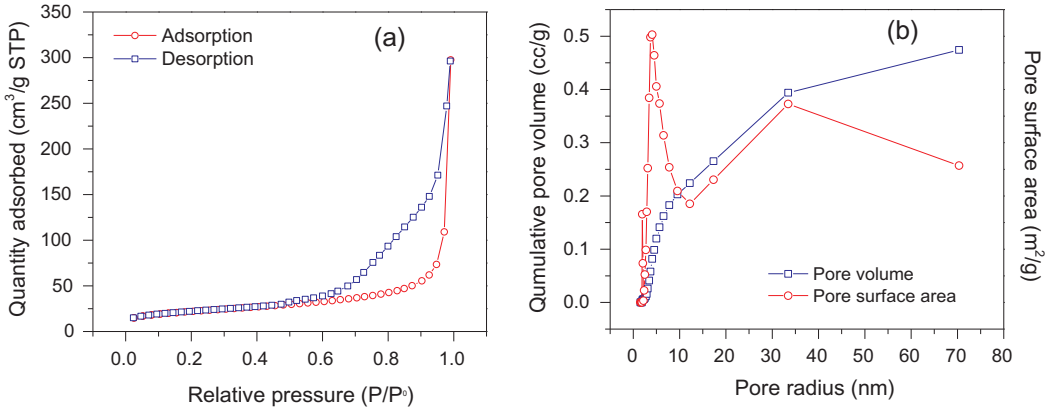

Fig. 6. Nitrogen adsorption-desorption isotherms at -196 °C and the corresponding average pore size distribution of Fe_3O_4@SiO_2-SO_3H nanoparticles.

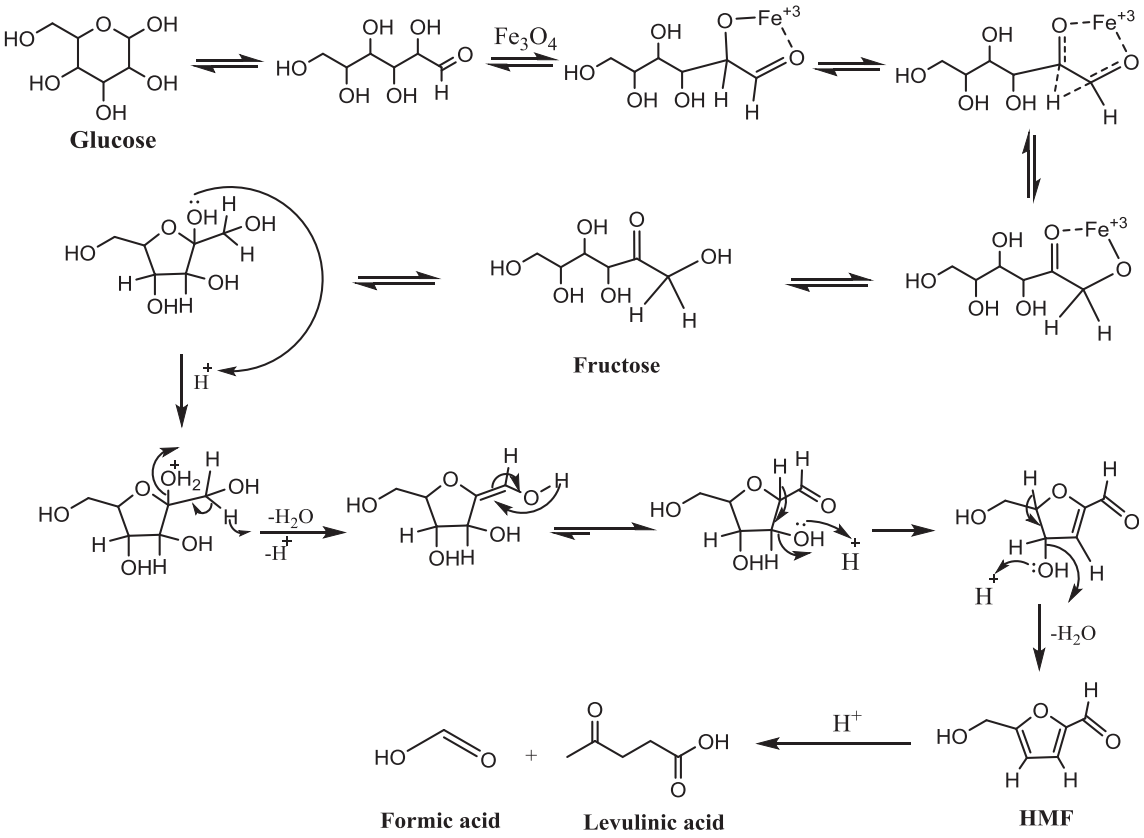

Scheme 1. Detailed mechanism for the isomerization and dehydration of glucose into HMF Ref. [51].

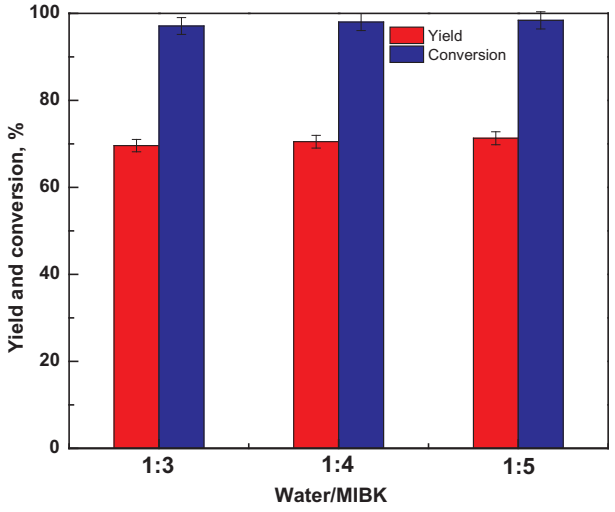

Fig. 7. Effect of water/MIBK ratio on HMF yield and glucose conversion (time = 24 h min; temperature = 140 °C; catalyst concentration = 40%).

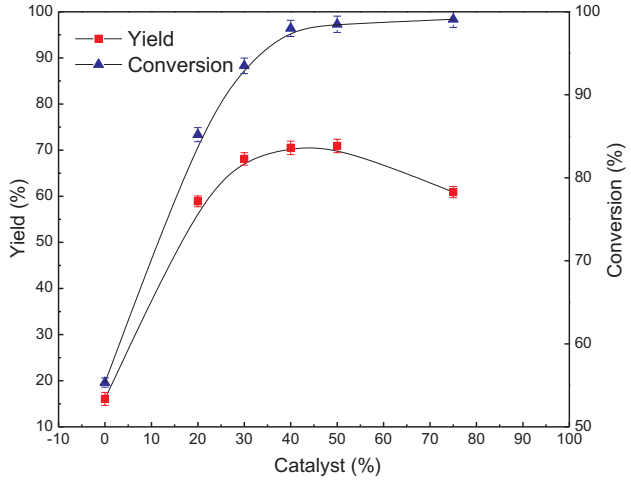

Fig. 8. Effect of catalyst concentration on HMF yield and glucose conversion (water/MIBK = 1:4; time = 24 h; temperature = 140 °C).

dehydration reactions of sugars to furan derivatives [55]. Several previous studies used high concentration of catalyst at different reaction times and temperatures to achieve high HMF yield. For example, Jiang et al. [54] used about 177% of formic acid catalyst (170 °C and 60 min) to produce 68.3% of HMF from fructose in aqueous/butanol media. Morales et al. [56] used 30 wt% of the 10Al-MCM catalyst with respect to glucose to achieve 87% of glucose conversion and 36% of HMF yield at 195 °C and 150 min in a biphasic water/MIBK system. Wang et al. [35] used 83.3% silica-coated MNPs supported phosphotungstic acid catalyst to achieve 64% yield of 5-ethoxymethylfurfural (EMF) for 9 h at 120 °C and 83.6% EMF yield for 11 h at 100 °C from fructose in ethanol. In this study, we aimed to determine the lowest catalyst concentration that can give the highest yield of HMF at the highest thermally stable catalyst temperatures (below 150 °C). Fig. 8 shows the effect of Fe_3O_4@SiO_2-SO_3H catalyst concentration on glucose conversion and HMF yield in (1:4) water/MIBK biphasic system at 140 °C temperature for 24 h. As shown on Fig. 8, the catalyst concentration had a pronounced effect on the yield of HMF. At 0% catalyst concentration, the yield of HMF was obviously low (16.0%) with 55.3% glucose conversion. The yield of HMF increased to 58.9% at 20% catalyst concentration, then slightly increased to 68.1% and 70.5% at 30 and 40% catalyst concentration, respectively. A further increase in catalyst concentration to 75% resulted in an obvious decrease in the yield of HMF to 60.9% due to the decomposition of HMF to levulinic and formic

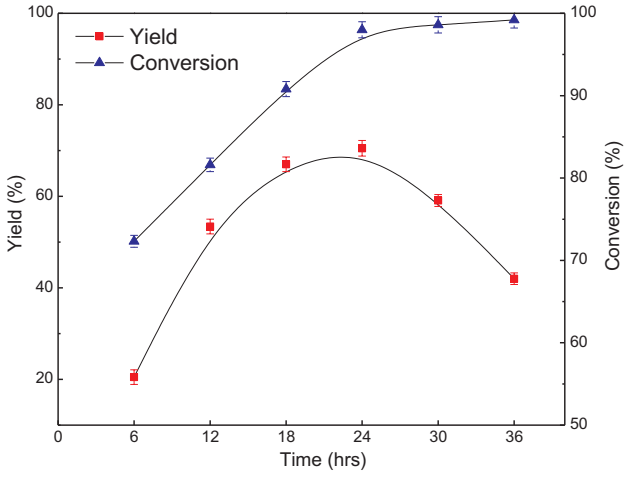

Fig. 9. Effect of time on HMF yield and glucose conversion (water/MIBK = 1:4; catalyst concentration = 40%; temperature = 140 °C).

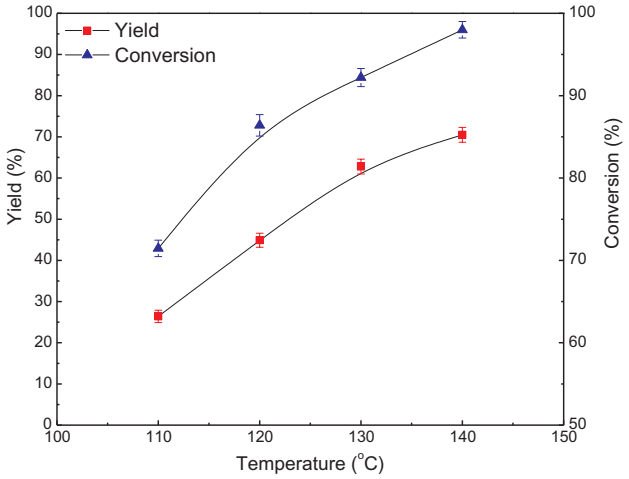

Fig. 10. Effect of reaction temperature on HMF yield and glucose conversion (water/MIBK = 1:4; catalyst concentration = 40%; time = 24 h).

acids by the acidic active sites on the catalyst surface. On the other hand, glucose conversion increased with the increase of catalyst concentration from 20 to 75%. High glucose conversion at high catalyst concentration may be attributed to the formation of undesirable by-products and humins at high catalyst concentration [54]. Therefore, the usage of 40% catalyst was selected as an optimum catalyst concentration for the next experiment. This catalyst concentration is considered to be considerably lower compared with the concentration of catalyst previously used to achieve comparable HMF yield. This result indicates high selectivity for the prepared catalyst towards the production of HMF.

3.5. Effect of reaction time and temperature on glucose dehydration process

Time and temperature are two important parameters affecting the yield of HMF. Applying higher temperature or longer reaction time can lead to a series of undesirable degradation byproducts [6]. According to previous studies, there is an inversely proportional relationship between time and temperature. Applying low reaction temperature is usually associated with prolonged reaction time and vice versa. In this study, we tried to optimize the production of HMF at relatively low temperatures (110–140 °C) and longer reaction time (6–36 h). Fig. 9 illustrates the effect of reaction time on the yield of HMF and glucose conversion; experiments were performed in (1:4) water/MIBK biphasic system at 140 °C and 40% catalyst concentration. As shown in Fig. 9, the conversion of glucose gradually increased from 72.3% to 98.0% with increasing time from 6 to 24 h then slightly increased to 99.2% at 36 h. The yield of HMF passed through three different stages. First, a sharp increase in the yield from (20.5 to 67%) between (6–18 h); then a slow increase in the yield until a maximum was reached (70.5%) at 24 h followed by a rapid decrease in the yield (42%) at 36 h. The drop in the yield of HMF after 36 h can be attributed to the decomposition of HMF to levulinic and formic acids under the given reaction conditions [6]. So, the optimum reaction time for the following experiments was chosen to be 24 h.

Fig. 10 shows the influence of reaction temperature on the yield of HMF yield and glucose conversion. It is clear from the figure that the increasing of temperature from 110 to 130 °C had a significant effect on both HMF yield and glucose conversion. The yield of HMF increased from 26.4 to 62.8% and the glucose conversion also increased from 71.5 to 92.2%. Increasing reaction temperature to 140 °C slightly improved the yield of HMF and glucose conversion to 70.5 and to 98%, respectively. It is obvious that any further increase in the temperature higher than 140 °C might lead to further increase in the yield of HMF. However, because the prepared catalyst is not thermally stable above 155 °C as concluded from TGA results, therefore, 140 °C was considered to be the optimum reaction temperature for this system.

3.6. Effect of DMSO on glucose dehydration process

The influence of phase modifiers in aprotic solvents such as DMSO in promoting the efficient production of HMF from carbohydrates was investigated in several previous studies [6,53,57]. The effect of a DMSO addition was recognized by suppressing the formation of condensation byproducts and hydration of furans produced in the reaction medium by lowering the water concentration in the aqueous phase. As a result, DMSO was added in this study to the aqueous phase to improve HMF yield and glucose conversion. Conversion experiments were performed at the optimum conditions previously determined (140 °C, 24 h and 40% catalyst concentration). Fig. 11 shows the effect of DMSO addition on HMF yield and glucose conversion, it is clear from the figure that addition of DMSO to the aqueous phase negatively affected the yield of HMF at all studied compositions. This result seems to disagree with the previous studies which indicated the positive effect of DMSO in suppressing the hydration of HMF into levulinic and formic acids [57]. In general, the positive effect of DMSO in suppressing the hydration reactions was obvious in relatively moderate strength acids such as formic acid [53]. In addition, DMSO itself can act as catalyst for dehydration of glucose to form HMF [57]. Presence of DMSO with the strong catalyst

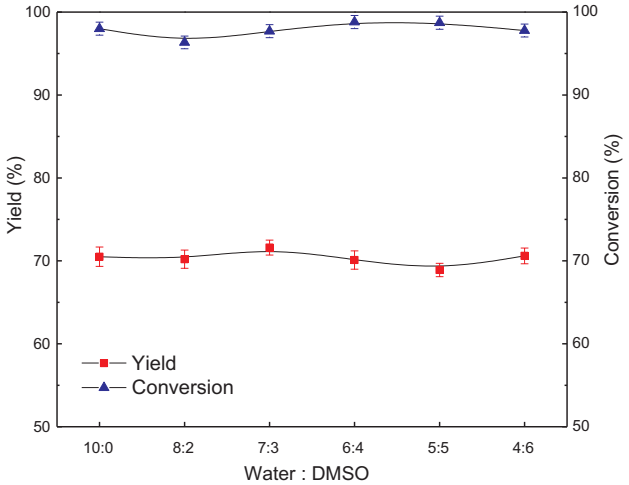

Fig. 11. Effect of DMSO addition on HMF yield and glucose conversion (water/MIBK = 1:4, catalyst concentration = 40%, time = 24 h, temperature = 140 °C).

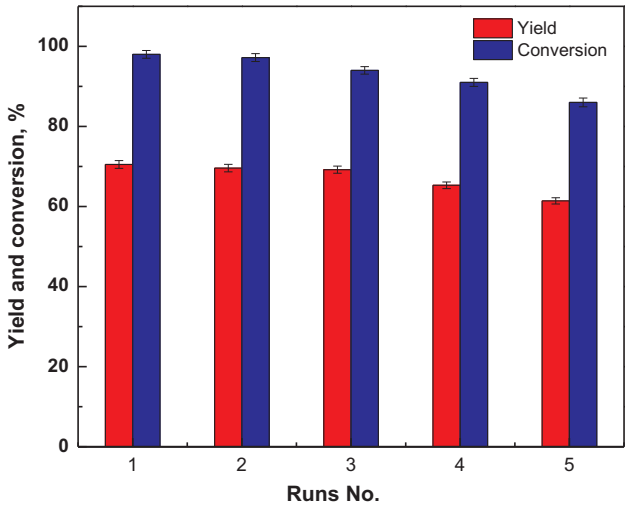

Fig. 12. Reusability test of the Fe_3O_4@SiO_2-SO_3H catalyst for the dehydration reaction of glucose (water/MIBK = 1:4; catalyst concentration = 40%; time = 24 h, temperature = 140 °C).

can increase the hydration of HMF as well. Therefore, the low yield of HMF in the presence of DMSO may be attributed to the high hydration strength of Fe_3O_4@SiO_2-SO_3H catalyst and this minimized the effect of DMSO in suppressing the hydration process. This result suggests that the effect of DMSO in suppressing hydration reactions and increasing the yield of HMF is not remarkable in the presence of very strong catalyst such as Fe_3O_4@SiO_2-SO_3H.

3.7. Catalyst reusability

The durability of the targeted magnetic nanoparticle catalyst was examined. Five recycling tests of Fe_3O_4@SiO_2-SO_3H catalyst at the optimum condition were performed. As shown in Fig. 12, the catalyst was stable for five runs without the loss of its catalytic activity. Clearly, the calculated yield of HMF reduced from 70.5 to 60.4 after five runs. The decrease in the HMF yield is attributed to two effects. The adsorption and accumulation of some oligomeric products on the sulfonic acid sites inside the pores of the catalyst leading to a substantial decrease in the catalyst reactivity [58,59]. It also may be related to the partial loss of SO_3H group from the surface of the spent catalyst as confirmed EDX analysis (Fig. 3) and acid-base titration curve (Fig. 4). The decrease in conversion (14.3%) is similar to the loss of sulfur (22%). The spent catalyst was used for the next run under the same reaction conditions. Each run was performed after washing and drying the catalyst.

4. Conclusion

A core-shell Fe_3O_4@SiO_2-SO_3H nanoparticle acid catalyst was successfully synthesized for dehydration of glucose to form HMF. The ability of this catalyst to act as Lewis and Brönsted acid represents new insight for the future application of this catalyst. The prepared catalyst showed a high catalytic activity for increasing glucose conversion and HMF yield. High HMF yield and glucose conversion were achieved by the application of (water/MIBK) biphasic system with Fe_3O_4@SiO_2-SO_3H as a catalyst. In this process, the addition of the catalyst and extracting phase (MIBK) increased the dehydration reaction efficiency of glucose and the HMF yield by limiting the HMF hydration side reaction and removing HMF from the reactive aqueous medium. The process variables, including catalyst concentration, reaction temperature and reaction time, had significant effects on glucose conversion and HMF yield. The optimum reaction conditions were found to be 40% catalyst concentration, 140 °C, 24 h, and the use of a biphasic system (water: MIBK) ratio of 1:4. Under such conditions, a glucose conversion of 98% with a HMF yield of 70.5% was achieved. The usage of 40% catalyst is considered to be very low compared with the concentration of catalyst previously used to achieve comparable HMF yield. The effect of DMSO in suppressing hydration reactions and increasing the yield of HMF was not remarkable in this study due to the presence of a very strong Fe_3O_4@SiO_2-SO_3H catalyst.

Acknowledgment

This study was supported by the Egyptian government predoctoral channel fellowship (Egyptian Missions sector) through Sustainable Bioproduct department at Mississippi State University for Mr. Islam Elsayed.

Appendix A. Supplementary data

Supplementary data associated with this article can be found, in the online version, at http://dx.doi.org/10.1016/j.fuel.2018.02.135.

References

[1] Isahak WNRW, Hisham MWM, Yarmo MA, Yun Hin T-Y. A review on bio-oil production from biomass by using pyrolysis method. Renew Sustain Energy Rev 2012;16(8):5910–23.
[2] Anbarasan P, Baer ZC, Sreekumar S, Gross E, Binder JB, Blanch HW, et al. Integration of chemical catalysis with extractive fermentation to produce fuels. Nature 2012;491(7423):235–9.
[3] Wilson K, Lee AF. Rational design of heterogeneous catalysts for biodiesel synthesis. Catal Sci Technol 2012;2(5):884–97.
[4] Somerville C, Youngs H, Taylor C, Davis SC, Long SP. Feedstocks for lignocellulosic biofuels. Science 2010;329(5993):790–2.
[5] Isikgor FH, Becer CR. Lignocellulosic biomass: a sustainable platform for production of bio-based chemicals and polymers. arXivorg, e-Print Arch, Condens Matter 2016:1–61.
[6] Román-Leshkov Y, Chheda JN, Dumesic JA. Phase modifiers promote efficient production of hydroxymethylfurfural from fructose. Science 2006;312(5782):1933–7.
[7] Mariscal R, Maireles-Torres P, Ojeda M, Sadaba I, Lopez Granados M. Furfural: a renewable and versatile platform molecule for the synthesis of chemicals and fuels. Energy Environ Sci 2016;9(4):1144–89.
[8] Yin S, Sun J, Liu B, Zhang Z. Magnetic material grafted cross-linked imidazolium based polyionic liquids: an efficient acid catalyst for the synthesis of promising liquid fuel 5-ethoxymethylfurfural from carbohydrates. J Mater Chem A 2015;3(9):4992–9.
[9] Xu S, Zhou P, Zhang Z, Yang C, Zhang B, Deng K, et al. Selective oxidation of 5-hydroxymethylfurfural to 2,5-furandicarboxylic acid using O2 and a photocatalyst of Co-thioporphyrazine bonded to g-C3N4. J Am Chem Soc 2017;139(41):14775–82.
[10] Alamillo R, Tucker M, Chia M, Pagan-Torres Y, Dumesic J. The selective hydrogenation of biomass-derived 5-hydroxymethylfurfural using heterogeneous catalysts. Green Chem 2012;14(5):1413–9.
[11] Rosatella AA, Simeonov SP, Frade RFM, Afonso CAM. 5-Hydroxymethylfurfural (HMF) as a building block platform: biological properties, synthesis and synthetic applications. Green Chem 2011;13(4):754–93.
[12] Zhang Z, Wang Q, Xie H, Liu W, Zhao Z. Catalytic conversion of carbohydrates into 5-hydroxymethylfurfural by germanium(IV) chloride in ionic liquids. ChemSusChem 2011;4(1):131–8.
[13] Zhang Y, Wang J, Li X, Liu X, Xia Y, Hu B, et al. Direct conversion of biomass-derived carbohydrates to 5-hydroxymethylfurural over water-tolerant niobium-based catalysts. Fuel 2015;139:301–7.
[14] Zhou P, Zhang Z. One-pot catalytic conversion of carbohydrates into furfural and 5-hydroxymethylfurfural. Catal Sci Technol 2016;6(11):3694–712.
[15] Chheda JN, Roman-Leshkov Y, Dumesic JA. Production of 5-hydroxymethylfurfural and furfural by dehydration of biomass-derived mono- and poly-saccharides. Green Chem 2007;9(4):342–50.
[16] Jiménez-Morales I, Santamaría-González J, Jiménez-López A, Maireles-Torres P. Glucose dehydration to 5-hydroxymethylfurfural on zirconium containing mesoporous MCM-41 silica catalysts. Fuel 2014;118:265–71.
[17] Nasirudeen MB, Hailes HC, Evans JRG. Preparation of 5-hydroxymethylfurfural from glucose and fructose in ionic liquids by reactive vacuum distillation over a solid catalyst. Curr Org Synth 2017;14(4):596–603.
[18] James OO, Maity S, Usman LA, Ajanaku KO, Ajani OO, Siyanbola TO, et al. Towards the conversion of carbohydrate biomass feedstocks to biofuels via hydroxylmethylfurfural. Energy Environ Sci 2010;3(12):1833–50.
[19] Pagán-Torres YJ, Wang T, Gallo JMR, Shanks BH, Dumesic JA. Production of 5-hydroxymethylfurfural from glucose using a combination of lewis and brønsted acid catalysts in water in a biphasic reactor with an alkylphenol solvent. ACS Catal 2012;2(6):930–4.

[20] Amarjargal A, Tijing LD, Im I-T, Kim CS. Simultaneous preparation of Ag/Fe3O4 core–shell nanocomposites with enhanced magnetic moment and strong antibacterial and catalytic properties. Chem Eng J 2013;226:243–54.
[21] Chen X, Arruebo M, Yeung KL. Flow-synthesis of mesoporous silicas and their use in the preparation of magnetic catalysts for Knoevenagel condensation reactions. Catal Today 2013;204:140–7.
[22] Liu B, Zhang Z. Catalytic conversion of biomass into chemicals and fuels over magnetic catalysts. ACS Catal 2016;6(1):326–38.
[23] Mei N, Liu B, Zheng J, Lv K, Tang D, Zhang Z. A novel magnetic palladium catalyst for the mild aerobic oxidation of 5-hydroxymethylfurfural into 2,5-furandicarboxylic acid in water. Catal Sci Technol 2015;5(6):3194–202.
[24] Zhang Z, Deng K. Recent advances in the catalytic synthesis of 2,5-furandicarboxylic acid and its derivatives. ACS Catal 2015;5(11):6529–44.
[25] Masala O, Seshadri R. Magnetic properties of capped, soluble MnFe2O4 nanoparticles. Chem Phys Lett 2005;402(1–3):160–4.
[26] Hyeon T, Lee SS, Park J, Chung Y, Na HB. Synthesis of highly crystalline and monodisperse maghemite nanocrystallites without a size-selection process. J Am Chem Soc 2001;123(51):12798–801.
[27] Sun S, Zeng H, Robinson DB, Raoux S, Rice PM, Wang SX, et al. Monodisperse MFe2O4 (M = Fe Co, Mn) Nanoparticles. J Am Chem Soc 2004;126(1):273–9.
[28] Cai W, Wan J. Facile synthesis of superparamagnetic magnetite nanoparticles in liquid polyols. J Colloid Interface Sci 2007;305(2):366–70.
[29] Qiao R, Yang C, Gao M. Superparamagnetic iron oxide nanoparticles: from preparations to in vivo MRI applications. J Mater Chem 2009;19(35):6274–93.
[30] Xu Z, Hou Y, Sun S. Magnetic core/shell Fe3O4/Au and Fe3O4/Au/Ag nanoparticles with tunable plasmonic properties. J Am Chem Soc 2007;129(28):8698–9.
[31] Deng Y, Deng C, Qi D, Liu C, Liu J, Zhang X, et al. Synthesis of core/shell colloidal magnetic zeolite microspheres for the immobilization of trypsin. Adv Mater 2009;21(13):1377–82.
[32] Morel A-L, Nikitenko SI, Gionnet K, Wattiaux A, Lai-Kee-Him J, Labrugere C, et al. Sonochemical approach to the synthesis of Fe3O4@SiO2 core − shell nanoparticles with tunable properties. ACS Nano 2008;2(5):847–56.
[33] Wang S, Tang J, Zhao H, Wan J, Chen K. Synthesis of magnetite–silica core–shell nanoparticles via direct silicon oxidation. J Colloid Interface Sci 2014;432:43–6.
[34] Santra S, Tapec R, Theodoropoulou N, Dobson J, Hebard A, Tan W. Synthesis and characterization of silica-coated iron oxide nanoparticles in microemulsion: the effect of nonionic surfactants. Langmuir 2001;17(10):2900–6.
[35] Wang S, Zhang Z, Liu B, Li J. Silica coated magnetic Fe3O4 nanoparticles supported phosphotungstic acid: a novel environmentally friendly catalyst for the synthesis of 5-ethoxymethylfurfural from 5-hydroxymethylfurfural and fructose. Catal Sci Technol 2013;3(8):2104–12.
[36] Xiong Y, Zhang Z, Wang X, Liu B, Lin J. Hydrolysis of cellulose in ionic liquids catalyzed by a magnetically-recoverable solid acid catalyst. Chem Eng J 2014;235:349–55.
[37] Wang J, Zhang Z, Jin S, Shen X. Efficient conversion of carbohydrates into 5-hydroxylmethylfurfan and 5-ethoxymethylfurfural over sufonic acid-functionalized mesoporous carbon catalyst. Fuel 2017;192:102–7.
[38] Park J, An K, Hwang Y, Park J-G, Noh H-J, Kim J-Y, et al. Ultra-large-scale syntheses of monodisperse nanocrystals. Nat Mater 2004;3(12):891–5.
[39] Zolfigol MA. Silica sulfuric acid/NaNO2 as a novel heterogeneous system for production of thionitrites and disulfides under mild conditions. Tetrahedron 2001;57(46):9509–11.
[40] Alemi-Tameh F, Safaei-Ghomi J, Mahmoudi-Hashemi M, Teymuri R. A comparative study on the catalytic activity of Fe3O4@SiO2–SO3H and Fe3O4@SiO2–NH2 nanoparticles for the synthesis of spiro [chromeno [2, 3-c] pyrazole-4, 3′-indoline]-diones under mild conditions. Res Chem Intermed 2016;42(7):6391–406.
[41] Rodulfo-Baechler SM, González-Cortés SL, Orozco J, Sagredo V, Fontal B, Mora AJ, et al. Characterization of modified iron catalysts by X-ray diffraction, infrared spectroscopy, magnetic susceptibility and thermogravimetric analysis. Mater Lett 2004;58(20):2447–50.
[42] Naeimi H, Nazifi ZS. A highly efficient nano-Fe3O4 encapsulated-silica particles bearing sulfonic acid groups as a solid acid catalyst for synthesis of 1,8-dioxo-octahydroxanthene derivatives. J Nanopart Res 2013;15(11):2026.
[43] Safari J, Zarnegar Z. A magnetic nanoparticle-supported sulfuric acid as a highly efficient and reusable catalyst for rapid synthesis of amidoalkyl naphthols. J Mol Catal A: Chem 2013;379:269–76.
[44] Shi-Yong Zhao DKL, Chang Woo Kim, Hyun Gil Cha, Young Hwan Kim, and Young Soo Kang. Synthesis of Magnetic Nanoparticles of Fe3O4 and CoFe2O4 and Their Surface Modification by Surfactant Adsorption. Bull Korean Chem Soc 2006;27(2):237–42.
[45] Mahdavi M, Ahmad M, Haron M, Namvar F, Nadi B, Rahman M, et al. Synthesis, surface modification and characterisation of biocompatible magnetic iron oxide nanoparticles for biomedical applications. Molecules 2013;18(7):7533.
[46] Sahoo Y, Pizem H, Fried T, Golodnitsky D, Burstein L, Sukenik CN, et al. Alkyl phosphonate/phosphate coating on magnetite nanoparticles: a comparison with fatty acids. Langmuir 2001;17(25):7907–11.
[47] Park J, An K, Hwang Y, Park JEG, Noh HJ, Kim JY, et al. Ultra-large-scale syntheses of monodisperse nanocrystals. Nat Mater 2004;3(12):891–5.
[48] Ding HL, Zhang YX, Wang S, Xu JM, Xu SC, Li GH. Fe3O4@SiO2 core/shell nanoparticles: the silica coating regulations with a single core for different core sizes and shell thicknesses. Chem Mater 2012;24(23):4572–80.
[49] Li J, Zhao H, Hou X, Fa W, Cai J. Fe3O4@SiO2-SO3H nanocomposites: an efficient magnetically separable solid acid catalysts for esterification reaction. IET Micro Nano Lett 2017;12(1):53–7.
[50] Choudhary V, Mushrif SH, Ho C, Anderko A, Nikolakis V, Marinkovic NS, et al. Insights into the interplay of lewis and brønsted acid catalysts in glucose and fructose conversion to 5-(Hydroxymethyl)furfural and levulinic acid in aqueous media. J Am Chem Soc 2013;135(10):3997–4006.
[51] Moreno-Recio M, Santamaría-González J, Maireles-Torres P. Brönsted and Lewis acid ZSM-5 zeolites for the catalytic dehydration of glucose into 5-hydroxymethylfurfural. Chem Eng J 2016;303(Supplement C):22–30.
[52] Dumesic JA, Pagán-Torres YJ, Wang T, Shanks BH. Lewis and bronsted-lowry acid-catalyzed production 5-hydroxymethylfurfural (HMF) from glucose. Google Patents; 2014.
[53] Abou-Yousef H, Hassan EB. Efficient utilization of aqueous phase bio-oil to furan derivatives through extraction and sugars conversion in acid-catalyzed biphasic system. Fuel 2014;137:115–21.
[54] Jiang N, Huang R, Qi W, Su R, He Z. Effect of formic acid on conversion of fructose to 5-hydroxymethylfurfural in aqueous/butanol media. Bioenerg Res 2012;5(2):380–6.
[55] McNeff CV, Nowlan DT, McNeff LC, Yan B, Fedie RL. Continuous production of 5-hydroxymethylfurfural from simple and complex carbohydrates. Appl Catal A 2010;384(1–2):65–9.
[56] Jiménez-Morales I, Moreno-Recio M, Santamaría-González J, Maireles-Torres P, Jiménez-López A. Production of 5-hydroxymethylfurfural from glucose using aluminium doped MCM-41 silica as acid catalyst. Appl Catal B 2015;164:70–6.
[57] Amarasekara AS, Williams LD, Ebede CC. Mechanism of the dehydration of d-fructose to 5-hydroxymethylfurfural in dimethyl sulfoxide at 150 °C: an NMR study. Carbohydr Res 2008;343(18):3021–4.
[58] Chen D, Liang F, Feng D, Xian M, Zhang H, Liu H, et al. An efficient route from reproducible glucose to 5-hydroxymethylfurfural catalyzed by porous coordination polymer heterogeneous catalysts. Chem Eng J 2016;300(Supplement C):177–84.
[59] Siril PF, Davison AD, Randhawa JK, Brown DR. Acid strengths and catalytic activities of sulfonic acid on polymeric and silica supports. J Mol Catal A: Chem 2007;267(1):72–8.